Available online at www.sciencedirect.com

ScienceDirect

Energy Procedia 137 (2017) 414–427

Energy Procedia

www.elsevier.com/locate/procedia

14th Deep Sea Offshore Wind R&D Conference, EERA DeepWind'2017, 18-20 January 2017, Trondheim, Norway

Spectral characteristics of surface-layer turbulence in the North Sea

Etienne Cheynet[a,*], Jasna Bogunović Jakobsen[a], Charlotte Obhrai[a]

[a]*Department of Mechanical and Structural Engineering and Materials Science, University of Stavanger, N-4036 Stavanger, Norway*

Abstract

According to IEC 61400-1 and IEC 61400-3 standards, the wind load on the rotor-nacelle assembly of offshore wind turbines should be estimated from the Kaimal or Mann spectral models, unless site-specific full-scale measurements are available. The Kaimal spectral model was developed in a flat and homogeneous onshore site and its applicability in offshore environment, e.g. the North Sea, where a number of wind turbines are in operation, is not thoroughly documented. The present paper utilizes the wind data recorded on the offshore platform FINO 1 in 2007 and 2008 to study the single-point auto-spectral and cross-spectral densities of wind turbulence. It investigates the validity of the Kaimal model, the Mann spectral model, the IEC Kaimal model and the one proposed in the NORSOK standard N-003. The latter standard is developed by the Norwegian petroleum industry for the design of offshore structures. Time series of 1 h duration are considered and a simple non-stationary wind model based on a time-varying fluctuating mean is used to increase the number of samples that can be treated as stationary.

For wind velocities ranging from 14 m s^{-1} to 28 m s^{-1}, a good agreement is observed between the Kaimal spectra and the measured ones, although the power spectral density of the wind fluctuations is larger than predicted for reduced frequencies below 0.04. The Mann spectral model showed a good agreement with the measured spectra. At the altitude of 80 m, we found in average $\Gamma = 3.7$, $\alpha\epsilon^{2/3} = 0.04\,\mathrm{m}^{4/3}\mathrm{s}^{-2}$ and $L = 70$ m. Finally, the NORSOK spectrum agrees fairly well with the measured one if a Charnock coefficient of 0.011 is used.

Peer-review under responsibility of SINTEF Energi AS.

Keywords: Surface-layer turbulence, FINO 1, Wind spectra, Full-scale measurements, Offshore wind

1. Introduction

The dynamic wind load on wind turbines is commonly modelled in the time domain using the wind spectral models provided by IEC 61400-1 [1]. These include the models by Kaimal et al. [2] and Mann [3], the parameters of which have been fitted to the Kaimal spectral model. The latter model was developed for a flat and homogeneous onshore site, and its applicability in offshore environment is little documented, especially for the North Sea. Few spectral models have been designed using offshore measurements. Among them is the wind spectrum currently used in the NORSOK standard [4] and developed based on field measurements in Sletringen (Frøya municipality), which is an island located ca. 110 km West of Trondheim in Norway.

* Corresponding author.
E-mail address: etienne.cheynet@uis.no

1876-6102
Peer-review under responsibility of SINTEF Energi AS.
10.1016/j.egypro.2017.10.366

The offshore platform FINO 1, located 45 km North of Borkum in Germany, provides continuous measurements of offshore wind since 2003 [5]. Until now, the data collected have been used to describe the turbulence intensity [6], to study the wind velocity profile over the sea [7], turbulent fluxes [8, 9] and the wind coherence [10]. The platform has also been utilized to investigate the applicability of wind lidar technology to measure turbulence statistics [11, 12]. As shown in a short review by Kettle [13], no in-depth analysis of the single-point auto-spectral and cross-spectral densities of the wind fluctuations has however been conducted.

Based on the wind data recorded on the offshore platform FINO 1 in 2007 and 2008, the present paper assesses the applicability of the Mann spectral model, the Kaimal spectral model and the NORSOK spectrum to model the surface-layer wind turbulence in offshore environment, under neutral and near-neutral atmospheric stability. The study is organized as follows: firstly, a review of measurements of offshore wind spectra during the last thirty years is presented. Secondly, the measurement site is briefly introduced as well as an overview of the wind conditions recorded in 2007 and 2008. Thirdly, the wind spectra estimated from the measurement data for the three wind components are compared to the Mann and the Kaimal spectral models. For the along-wind component, the comparison also includes the NORSOK spectrum and the IEC Kaimal spectrum. The discussion focuses on the challenges associated with the study of the spectral characteristics of offshore wind.

2. Instrumentations and methods

2.1. A review of offshore wind spectra

At the end of the 70s, Naito [14, 15] conducted early measurements of the spectral characteristics of offshore wind in Japan, 1 km from the coast and up to 15 m above sea level. These measurements remain a rare case where the three wind components were measured offshore (Table 1). In 1985, based on the measurements of Smith [16], Kareem [17] proposed an empirical wind spectrum for the along-wind component derived from Kaimal et al. [2] that was better suited for modelling the dynamic wind loads in offshore environment. In 1988, Ochi et al. [18] reviewed the different wind spectra measured the decade before and showed that they were similar in the high frequency domain but displayed significant differences in the low frequency range, which highlights the need to use site-specific spectra to better model wind loads on offshore structures. In the 90s, the spectral characteristics of wind were studied on the Norwegian coast by Andersen and Løvseth [19–21] and are currently used in NORSOK Standard [4]. More recently, the de Maré and Mann [22] assessed the Mann turbulence model in the Baltic Sea for wind velocities ranging from $8\,\mathrm{m\,s^{-1}}$ to $12\,\mathrm{m\,s^{-1}}$. The present paper complements their study by considering larger wind velocities and a higher measurement altitude.

In the present study, the along-wind, across-wind and vertical wind component are denoted u, v and w, respectively. The wind component $i = \{u, v, w\}$ is a random process that can be split up into a mean part, $\overline{i}$, and a fluctuating part with zero mean, i'. By definition, $\overline{v} = \overline{w} = 0\,\mathrm{m\,s^{-1}}$ [23], leading to the following relations:

$$u = \overline{u} + u' \tag{1}$$

$$v = v' \tag{2}$$

$$w = w' \tag{3}$$

Table 1. Review of full-scale measurements of offshore wind spectral densities.

Reference	Location	Wind component(s)	Velocity range	Averaging time
Naito [14, 15]	Sagami Bay	u, v, w	$2\,\mathrm{m\,s^{-1}} < \overline{u} < 19\,\mathrm{m\,s^{-1}}$	27 min
Smith [16], Kareem [17]	Atlantic NW	u	$6\,\mathrm{m\,s^{-1}} < \overline{u} < 22\,\mathrm{m\,s^{-1}}$	40 min
Eidsvik [24]	Norwegian Sea	u	$2\,\mathrm{m\,s^{-1}} < \overline{u} < 36\,\mathrm{m\,s^{-1}}$	20 min
Andersen and Løvseth [21]	Norwegian Sea	u	$15\,\mathrm{m\,s^{-1}} < \overline{u} < 27\,\mathrm{m\,s^{-1}}$	40 min
de Maré and Mann [22]	Baltic Sea	u, v, w	$8\,\mathrm{m\,s^{-1}} < \overline{u} < 12\,\mathrm{m\,s^{-1}}$	30 min
Present study	North Sea	u, v, w	$14\,\mathrm{m\,s^{-1}} < \overline{u} < 28\,\mathrm{m\,s^{-1}}$	60 min

Table 1 summarizes the former measurement campaigns focusing on the spectral analysis of the turbulent wind, a majority of which were conducted more than 25 years ago. Focus has often been on the along-wind component u only. Yet, the application of the Mann turbulence model requires the knowledge of the auto-spectra of the three wind components, denoted S_u, S_v and S_w as well as the cross-spectrum between the along-wind and vertical wind component S_{uw}. The present paper investigates therefore the spectral characteristics of all three wind components.

2.2. Data processing

Table 1 shows that the averaging time used in the previous studies varied between 20 min and 40 min. For a stationary random process, a larger averaging time leads in general to an increased accuracy of the estimated turbulence statistics [25, Chap. 1.15]. Offshore environments may be characterized by the predominance of unstable atmospheric conditions [26, 27] for which the turbulent time scales are larger than for the neutral atmosphere, requiring the use of averaging time larger than the standard value of 10 min. Similarly to Kaimal et al. [2], we chose to use an averaging time of 60 min in the present study, which is also the averaging time adopted in ESDU 86010 [28]. This allows in addition the application of the non-stationary wind model used by e.g. Xu and Chen [29] and Chen et al. [30] which relies on the idea that wind statistics may slowly fluctuate with time. If a sample duration of 10 min is used, these fluctuations cannot be properly captured. The first non-stationary model, refereed to as model I by Xu and Xia [31], describes the wind velocity data as the superposition of a time-varying mean and a stationary wind fluctuating component. The time-varying mean is estimated by applying the empirical mode decomposition (EMD) [32]. The stationarity of the remaining fluctuating component is assessed using the stationary test from Bendat and Piersol [33]. This test is conducted using 900 reverse arrangements per hour and a 95% confidence interval. The EMD algorithm used in the present study comes from Flandrin et al. [34]. After application of the EMD and the removal of any linear trend, between 20 % and 30 % of the samples were detected as non-stationary per month. The non-stationary model II relies on the use of a time-varying wind spectrum, also called evolutionary power spectral density (EPSD) [35–37]. This model is not investigated in the present paper, although it may become central for floating wind turbines for which the combined effects of wind and waves are commonly studied using different averaging times. For example, IEC 61400-1 [1] advises an averaging time of 10 min for the wind and 3 h for the waves. As shown by e.g. Wang et al. [38], the probability to measure stationary winds with an averaging time of 3 h may be close to zero, calling for the application of the non-stationary wind model II.

After disregarding non-stationary wind records, the single-point auto and cross-spectra are calculated using Welch's algorithm [39] with 4 segments of 15 min duration and 50% overlapping. The wind spectra are afterwards segregated into 6 bins corresponding to wind velocities ranging from 14 m s^{-1} to 28 m s^{-1}, which largely overlaps the typical wind velocity range for the rated output power of a wind turbine [40]. The median of the wind spectra is then calculated for each velocity bin instead of the mean value to reduce the influence of possible outliers on the averaged spectra.

2.3. The FINO 1 platform

The FINO 1 met-mast is a 81 m long steel lattice tower installed on a 20 m high jacket platform at 28 m water depth. It is instrumented with 8 cup anemometers (CA) at heights ranging from 33 m to 100 m, 4 wind vanes at heights between 33 m and 90 m and 3 Gill R3-50 sonic anemometers (SA) operating at 40 m, 60 m and 80 m [41]. In the present study, only the data recorded by the SA located 80 m above sea level is used.

2.4. Spectral models

2.4.1. Blunt and pointed models

The general expression of the wind spectrum $S(f)$ can be given as a function of the friction velocity u_*, the altitude z, the mean wind velocity $\overline{u}$ and 6 floating parameters a, b, c, α, β and γ [42, 43]:

$$\frac{fS(f)}{u_*^2} = \frac{an^\gamma}{(c + bn^\alpha)^\beta} \tag{4}$$

$$n = \frac{fz}{\overline{u}} \tag{5}$$

Table 2. Parameters a_i and b_i, $i = \{u, v, w\}$ used in the Kaimal spectral model.

	u	v	w	uw
a_i	105	17	2.1	14
b_i	33	9.5	5.3	9.6

where n is the reduced frequency. The friction velocity u_* is calculated following the definition given by Weber [44]:

$$u_* = \left(\overline{uw}^2 + \overline{uv}^2\right)^{1/4}. \tag{6}$$

The relationship between the friction velocity and the variance of the wind components is given through the so-called "turbulence intensity factor" β_i ($i = \{u, v, w\}$):

$$\sigma_i^2 = \beta_i u_*^2. \tag{7}$$

According to Tieleman [43], $\alpha = 1, \beta = 5/3, \gamma = 1$ and $c = 1$ (the so-called "blunt model") is recommended for perturbed terrain whereas $\alpha = 5/3, \beta = 1, \gamma = 1$ and $c = 1$ ("pointed model") is representative of flat, smooth and uniform terrains. As summarized by Solari and Piccardo [45], the "pointed model" and the "blunt model" are the most common wind spectral models found in the literature. In both models, a and b are the two remaining floating parameters in the wind spectrum. Kaimal et al. [2] used the "blunt model" for the horizontal components (Eqs. 8-9) but the "pointed model" for the vertical component:

$$\frac{fS_u}{u_*^2} = \frac{a_u n}{(1 + b_u n)^{5/3}} \tag{8}$$

$$\frac{fS_v}{u_*^2} = \frac{a_v n}{(1 + b_v n)^{5/3}} \tag{9}$$

$$\frac{fS_w}{u_*^2} = \frac{a_w n}{1 + b_w n^{5/3}} \tag{10}$$

$$\frac{fS_{uw}}{u_*^2} = -\frac{a_{uw} n}{(1 + b_{uw} n)^{2.4}} \tag{11}$$

where a_i and b_i, $i = \{u, v, w, uw\}$ are defined in Table 2.

To provide a consistent comparison between the coefficients a_i and b_i found by the Kaimal spectral model and those found using the data recorded at the FINO 1 platform, we chose to proceed in a similar fashion as Kaimal et al. [2], i.e. by using the "blunt model" for S_u and S_v and the "pointed model" for S_w. For the cross-spectrum S_{uw}, we use a similar spectrum as by Kaimal et al. [2], i.e. with $\alpha = 1, \beta = 2.4, \gamma = 1$ and $c = 1$.

2.4.2. The Mann spectral model

The Mann spectral model [3, 46] is more complex compared to the spectral models used in subsection 2.4.1 and will not be described explicitly here for the sake of brevity. Although the along-wind component is of major interest for offshore structures, the application of the Mann turbulence model requires the knowledge of the three turbulent components as well as the real part of the cross-spectrum S_{uw}. The Mann spectral model depends on three parameters $\alpha\epsilon^{2/3}$, L and Γ. The term $\alpha\epsilon^{2/3}$ is a measure of the energy dissipation, where ϵ is the rate of viscous dissipation of specific turbulent kinetic energy and α is the three-dimensional Kolmogorov constant equal to 1.7. L is a length scale of the spectral velocity tensor and Γ is the shear parameter that quantifies the anisotropy of the spectral tensor. In the present paper, $\alpha\epsilon^{2/3}$, L and Γ are floating parameters that are estimated by fitting the Mann spectral model to S_u, S_v and S_w as well as the real part of the cross-spectral density S_{uw}.

2.4.3. The NORSOK and IEC Kaimal models

The so-called "Frøya model" [19–21] is used in the NORSOK Standard [4] to model the wind spectrum of the along-wind component only. It is defined using the mean wind velocity $\overline{u}_r$ measured 10 m above sea level and the target

altitude z:

$$S_u(f) = 320\left(\frac{\overline{u}_r}{10}\right)^2\left(\frac{z}{10}\right)^{0.45}(1+A^m)^{-\frac{5}{3m}} \tag{12}$$

$$A = 172f\left(\frac{\overline{u}_r}{10}\right)^{-0.75}\left(\frac{z}{10}\right)^{2/3} \tag{13}$$

$$m = 0.468 \tag{14}$$

where $\overline{u}_r$ is defined using the logarithmic profile:

$$\overline{u}_r = \frac{u_*}{\kappa}\ln\left(\frac{10}{z_0}\right); \quad \kappa = 0.4 \tag{15}$$

and z_0 is estimated using the Charnock relation [47]:

$$z_0 = \frac{a}{g}u_*^2; \quad g = 9.81\,\mathrm{m/s^2}, \quad a = 0.0172 \tag{16}$$

The IEC Kaimal spectral model [1] for the along wind component is defined as:

$$\frac{fS_u(f)}{\sigma_u^2} = \frac{4fL_u/\overline{u}}{(1+6fL_u/\overline{u})^{5/3}} \tag{17}$$

$$L_u = 8.1\Lambda_1 \tag{18}$$

$$\Lambda_1 = \begin{cases} 0.7z & \text{if } z \le 60\,\mathrm{m} \\ 42\mathrm{m} & \text{if } z \ge 60\,\mathrm{m} \end{cases} \tag{19}$$

Contrary to the Kaimal or the Mann spectral model that are by definition normalized with respect to u_*^2, the IEC Kaimal model for the along-wind component is normalized by σ_u^2 and the NORSOK spectrum is not normalized. This may introduce additional discrepancies between the measured spectra and these models.

2.5. Atmospheric stability

The present study focuses on two years of wind records from 2007 to 2008. Fig. 1 shows that the years 2007 and 2008 may be considered as representative of wind condition in the North Sea during the last 27 years. The stacked bar plot in Fig. 1 is made using wind data recorded at the Ekofisk oil field in the North Sea from 1990 to 2017 (1.2×10^5 samples). These data have been obtained using the access-free database from the Norwegian Meteorological Institute [48] and corresponds to the 10 min mean wind velocity 10 m above sea level, stored every three hours.

During the year 2008, we did not have access to temperature measurements obtained at the FINO 1 platform. The atmospheric stability conditions were therefore assessed based on the spectral estimates, following the approach of

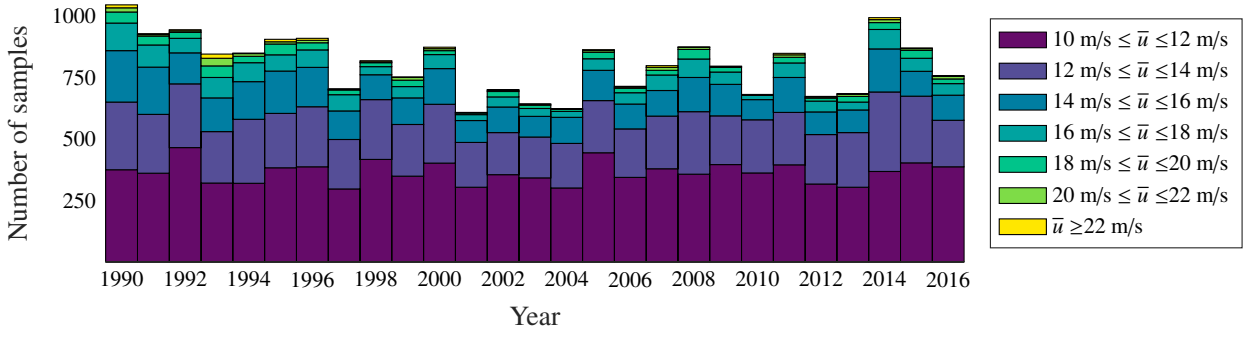

Fig. 1. Number of wind records bounded between 10 m s^{-1} and 24 m s^{-1} at the Ekofisk oil field from 1990 to 2017.

Kaimal et al. [2], who studied the ratio S_w/S_u as a function of the reduced frequency n and the dimensionless Obukhov stability parameter z/L. According to the theory of isotropic turbulence, the ratio $S_w/S_u = 4/3$ is expected in the inertial subrange. For neutral stability, Kaimal et al. [2] observed that the ratio was relatively constant and equal to $4/3$ for $n \geq 2$, then decreased monotonically to reach a ratio of $S_w/S_u = 1$ for $n \simeq 0.75$. In the present case, only samples satisfying $1.2 \leq S_w/S_u \leq 1.4$ for $2 \leq n \leq 5$ and $0.9 \leq S_w/S_u \leq 1.1$ for $0.5 \leq n \leq 1$ are selected as representative of a relatively neutral atmospheric stability. By doing so, at least 80% of the wind samples were disregarded. This is relatively consistent several studies [26, 27] who found that the marine boundary layer may be neutral only about 20 % of the time, or even less [49].

3. Results and discussions

3.1. Wind conditions at the FINO 1 platform in 2007-2008

A summary of the wind conditions measured at FINO 1, 80 m above the sea is given in Fig. 2. For the sake of clarity, the wind rose on the left panel is displayed for hourly wind velocities above 14 m s^{-1} only. Wind records obtained for a mean direction ranging from 90° to 160° have been disregarded as they are located in the mast shadow [50]. Data recorded with a wind direction between 60° and 90° shows however that the mast shadow may cover an area larger than predicted. During the measurement period from 2007-2008, the largest wind velocities were recorded for a direction ranging from South to West, with an average turbulence intensity (TI) rarely above 10% as shown in the right panel of Fig. 2. The measured values of I_u and their relation to the predicted values in IEC61400-3 [51] is consistent with the observations from Türk and Emeis [6] where the increased surface roughness is estimated based on the Charnock relation [47]. In Fig. 2, the ratio I_v/I_u and I_w/I_u are equal to 0.77 and 0.53 respectively for $\overline{u} > 15$ m s^{-1}, which is in the range of expected values [45].

The estimation of β_i ($i = \{u, v, w\}$) is more challenging because a relatively large scatter is measured, except for the vertical component. A value commonly used for β_u ranges from 6.1 to 6.5 [16, 52], although Solari and Piccardo [45] reviewed values ranging from 5 to more than 12 for $z_0 < 0.01$ m. Fig. 3 shows the histogram of β_i based on 1 h wind velocity data recorded in 2007-2008 at the FINO 1 platform ($z = 80$ m) after disregarding non-stationary samples and

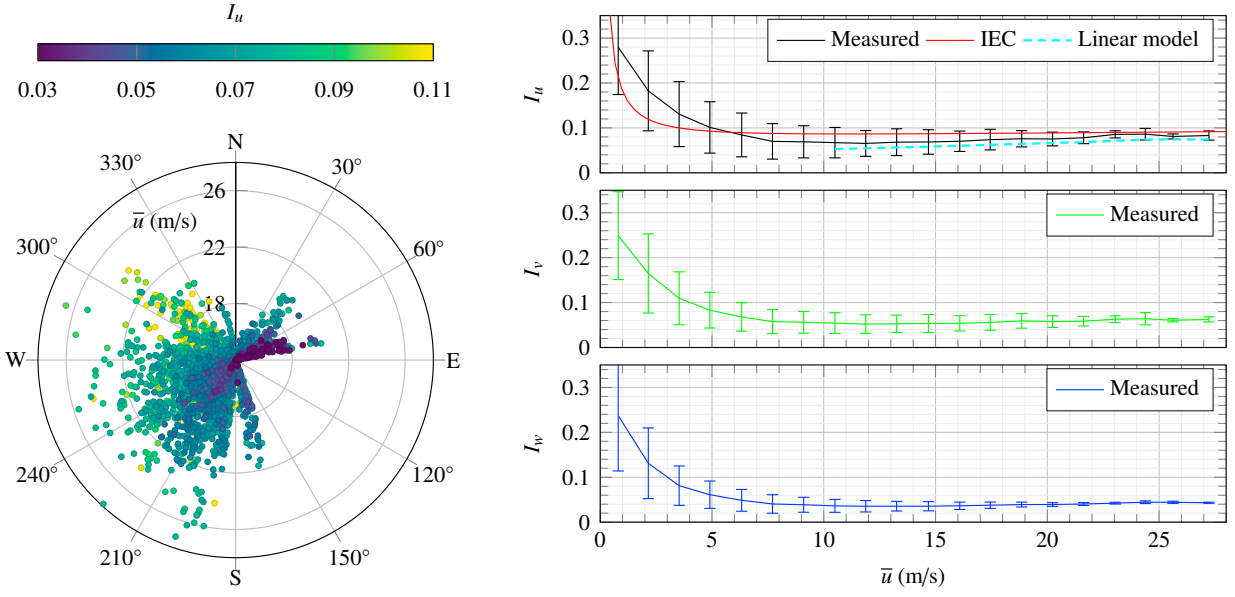

Fig. 2. Left:Wind rose made of 1 h wind velocity data over 14 m s^{-1} recorded during the year 2007-2008 at the FINO 1 platform, 80 m above sea level (2.8×10^3 samples). Right: Hourly turbulence intensity recorded during the year 2007-2008 80 m above the sea level at the FINO 1 platform, after pre-processing, and comparison with the predicted value given in IEC61400-3 [51] for a hub height of 80 m and the linear model from Andersen and Løvseth [21].

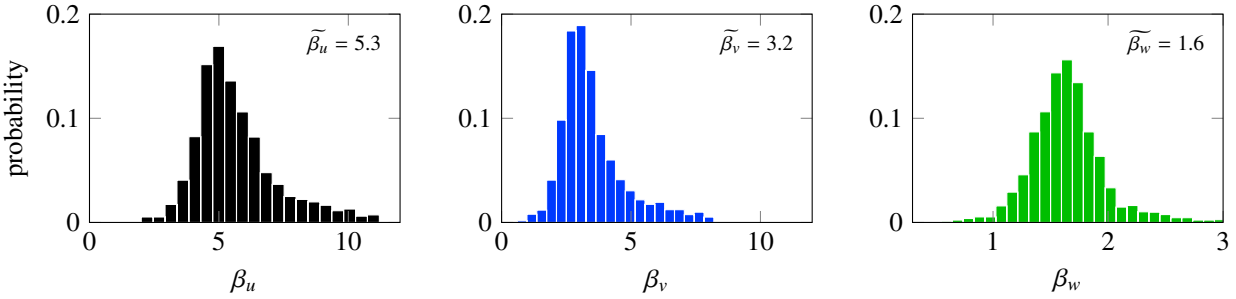

Fig. 3. Histograms of the turbulence intensity factor recorded at the FINO 1 platform during the year 2007-2008, based on 1 h wind velocity data over 14 m s^{-1} and disregarding data above the 75$^{\text{th}}$ percentile (2.8×10^3 samples) to improve the readability of the histograms.

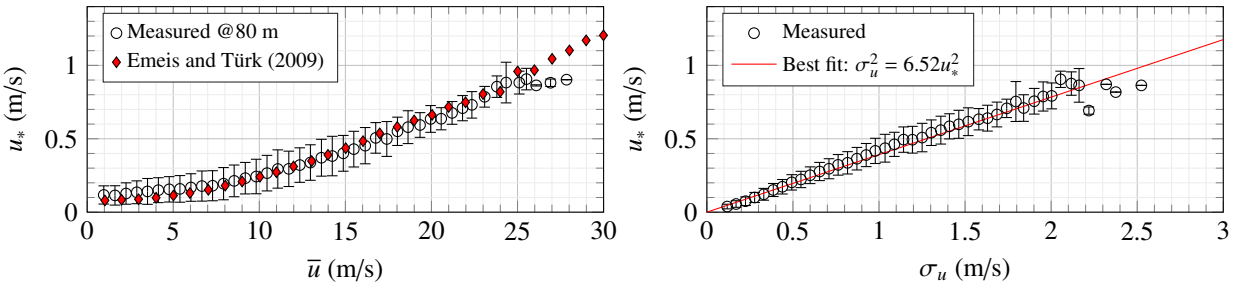

Fig. 4. Evolution of the hourly friction velocity with $\overline{u}$ (left) and σ_u (right) in 2007-2008, 80 m above the sea level at the FINO 1 platform, after removal of non-stationary samples. For the right panel, only samples characterized by $I_u < 0.1$ have been considered.

considering samples with a wind velocity over 14 m s^{-1} only. To improve the readability of the histograms displayed in Fig. 3, values of β_i above the 75$^{\text{th}}$ percentile were disregarded. If the values above the 75$^{\text{th}}$ are included, the median values of the turbulence intensity factors are $\widetilde{\beta_u} = 5.5$, $\widetilde{\beta_v} = 3.3$ and $\widetilde{\beta_w} = 1.6$, which is hardly larger than the median values displayed in Fig. 3. In Fig. 4, the variation of u_* with $\overline{u}$ agrees rather well with the results by Emeis and Türk [9], which concerned a larger data set measured 40 m above sea level. For high wind velocities, the present data indicates a slower increase in the implied surface drag coefficient with wind velocity, similarly to the data by Andersen and Løvseth [21]. By considering only samples verifying $I_u \leq 10\,\%$, the evolution of u_* with σ_u is almost linear and a linear regression gives $\beta_u = 6.5$. The non-linearity becomes however more pronounced for $\sigma_u \geq 2$ m s^{-1}.

3.2. Comparison with the Kaimal spectrum model

For six velocity bins ranging from 14 m s^{-1} to 28 m s^{-1}, the single point auto-spectra and the real part of the cross-spectrum Re$\{S_{uw}\}$ are calculated based on the hourly wind data recorded during 2007-2008 by the Sonic anemometer at $z = 80$ m. For each velocity bin, the high-frequency content of the averaged measured spectra is smoothed using a logarithmically spaced interval, facilitating the comparison with the predicted spectra. The estimated normalized spectra are similar for the six wind velocity intervals considered. More noisy spectra are however obtained for wind velocities above 22 m s^{-1} as the number of samples acquired at such large velocities is relatively low.

The fitted Kaimal spectra S_u, S_v and S_w agree remarkably well with the measured ones. These observations are consistent with low level airborne measurements conducted by Nicholls and Readings [53] over the sea outside of UK. For $n < 0.04$ and for every velocity bin, the fitted spectrum S_u shows in the present study a slightly lower energy content than measured. To further access the discrepancies, the blunt model and the pointed model presented in Eqs. 8-11 were fitted to the measured spectra in the least-square sense. Fig. 6 shows the measured and fitted spectra whereas Fig. 7 displays the estimated values of a_i and b_i ($i = \{u, v, w, uw\}$) as a function of the binned mean wind velocity. In Fig. 7, the solid lines correspond to the coefficients found by Kaimal et al. [2] whereas the fitted coefficients found for the FINO 1 platform at $z = 80$ m are displayed as marks. The fitted coefficients a_u and b_u range from 129 to 239 and from 36 to 63, respectively. The estimated values of a_u and b_u are relatively constant, except for the fifth velocity bin,

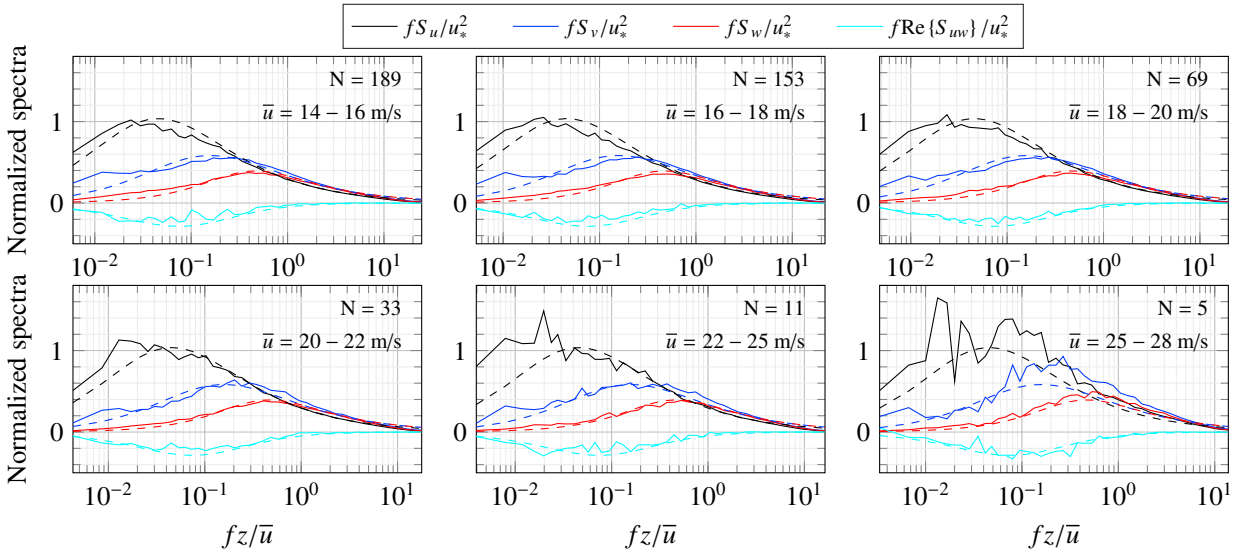

Fig. 5. Wind spectra measured (solid lines) and the Kaimal spectra (dashed lines) based on 1 h stationary wind data recorded at the FINO 1 platform, 80 m above sea level. The number of averaged samples is denoted by N in each panel.

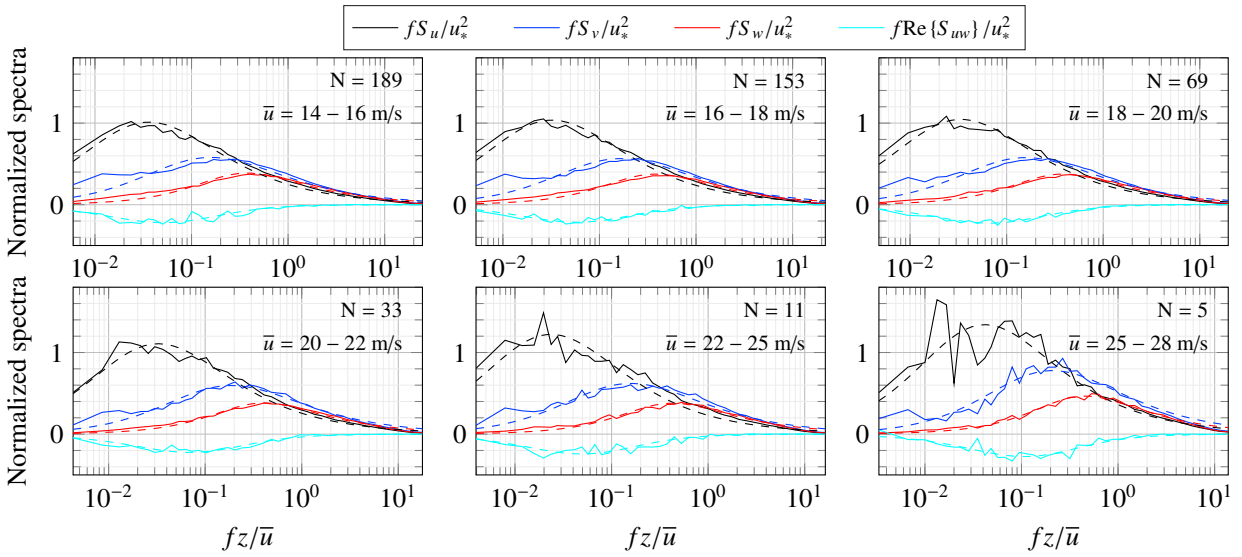

Fig. 6. Wind spectra measured (solid lines) and fitted spectra according to Eq. 4 (dashed lines) based on 1 h stationary wind data recorded at the FINO 1 platform, 80 m above sea level.

i.e. for $22\,\mathrm{m\,s^{-1}} \leq \overline{u} \leq 25\,\mathrm{m\,s^{-1}}$, where the value of the estimated coefficients may be outliers. The coefficients a_v, b_v, a_w and b_w are all consistent and show little dependency on the mean wind velocity $\overline{u}$. The coefficients a_{uw} and b_{uw} are however slightly decreasing for an increasing wind velocity. In a first approximation, the dependency of a_{uw} and b_{uw} on the mean wind velocity is however considered small enough so that the median of a_{uw} and b_{uw} can be estimated in the velocity range $14\,\mathrm{m\,s^{-1}} \leq \overline{u} \leq 28\,\mathrm{m\,s^{-1}}$.

The median values of a_i and b_i ($i = \{u, v, w, uw\}$), based on all velocity bins, denoted $\widetilde{a_i}$ and $\widetilde{b_i}$ respectively, are presented in Table 3. If the fifth velocity bin is excluded, the values are more or less the same. An alternative approach to estimate $\widetilde{a_i}$ and $\widetilde{b_i}$ may be to apply a weighted median accounting for the different number of samples in the different

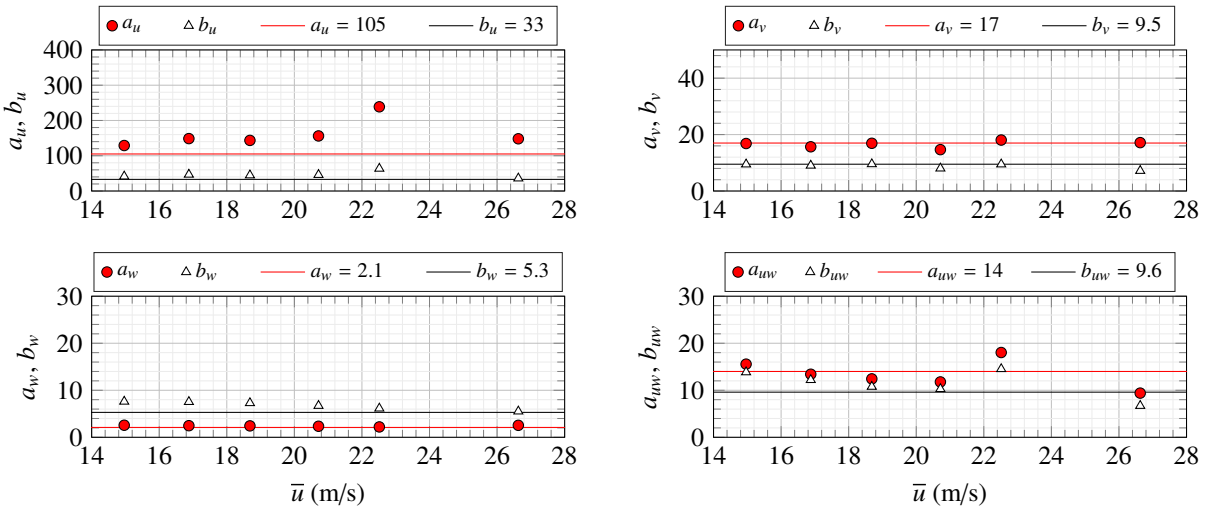

Fig. 7. Coefficients a_i and b_i ($i = \{u, v, w, uw\}$) estimated after least-square fitting of the blunt and pointed spectral models to the measured single-point spectra recorded at the FINO 1 platform, 80 m above sea level in 2007-2008. The coefficients presented in Table 2 are shown as solid lines.

Table 3. Median value of the fitted coefficients for the six velocity bins considered in Fig. 7.

Operator	$\widetilde{a_u}$	$\widetilde{b_u}$	$\widetilde{a_v}$	$\widetilde{b_v}$	$\widetilde{a_w}$	$\widetilde{b_w}$	$\widetilde{a_{uw}}$	$\widetilde{b_{uw}}$
Median	148	45	17	9.3	2.5	7.0	13	12
Weighted median	144	45	17	9.5	2.5	7.5	13	12

velocity bins. Such an approach gives a slightly lower value for $\widetilde{a_u}$ whereas the remaining coefficients are more or less unchanged.

As expected, the values of $\widetilde{a_u}$ and $\widetilde{b_u}$ are those which differ most from those in Table 2. The variance of the along-wind component calculated using $a_u = 148$ and $b_u = 45$ is ca. 17 % larger than if $a_u = 105$ and $b_u = 33$ are used. Although the values of $\widetilde{a_u}$ and $\widetilde{b_u}$ are larger than those found by Kaimal et al. [2], they remain lower than those found by Kareem [17], which are $a_u = 335$ and $b_u = 71$. A least-square fit of Eq. 8 to the Ochi spectrum [18] leads to even larger coefficients a_u and b_u, with $a_u \simeq 810$ and $b_u \simeq 120$ respectively. On the other hand, the Simiu and Scanlan spectrum [54] is relatively close to the one discussed in the present study, with $a_u = 200$ and $b_u = 50$.

3.3. Comparison with the fitted Mann spectral model

The Mann spectral model requires only 3 parameters whereas Eqs. 8-11 involve a total of 8 parameters. On the other hand, the parameters of the Mann turbulence model vary with the altitude and the mean wind velocity [46]. As shown in Fig. 9, we chose here to fit the Mann spectral model to the measured spectra directly, rather than to use values previously calculated in e.g. Mann [46]. In Fig. 8, the comparison of the fitted Mann spectral model to the measured spectra shows a good agreement for different velocities bins. The spectral peak for S_u is properly captured, although the fitted spectra remains slightly below the measured one at reduced frequency below 0.02, whereas the computed real part of S_{uw} is slightly larger in magnitude than measured. The parameters of the fitted model are relatively stable for the different velocity bins (Fig. 9), with a median value for Γ, $\alpha\epsilon^{2/3}$ and L equal to 3.7, 0.04 $\mathrm{m}^{4/3}\mathrm{s}^{-2}$ and 70 m respectively.

For the ESDU model spectra [28] computed over the sea, Mann [46] provided a chart where the values of $\alpha\epsilon^{2/3}$, L and Γ can be estimated given $\overline{u}$ and the altitude z. For $\overline{u} = 20\,\mathrm{m\,s^{-1}}$ and $z = 80$ m, one reads $\alpha\epsilon^{2/3} \simeq 0.19\,\mathrm{m}^{4/3}\mathrm{s}^{-2}$, $L \simeq 55$ m and $\Gamma \simeq 4.5$. The values we obtained in the present case are slightly different. In a more recent study, de Maré and Mann [22] fitted the Mann spectral model to the wind spectra recorded at Rødsand II offshore wind farm in the Baltic Sea, for altitudes ranging from 15 m to 57 m and wind velocities from 8 $\mathrm{m\,s^{-1}}$ to 12 $\mathrm{m\,s^{-1}}$ at 15 m above sea level. Although the SA they used at 15 m above sea level was likely located close to or in the "wave disturbed layer" [55], the

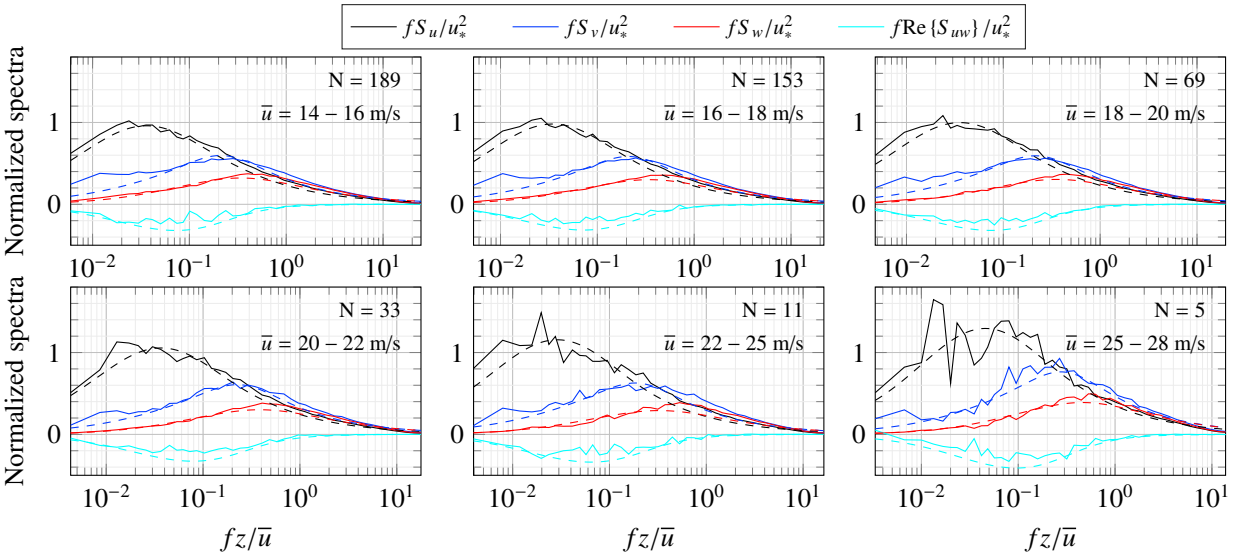

Fig. 8. Wind spectra measured (solid lines) and fitted using the Mann spectral model (dashed lines) based on 1 h stationary wind data recorded at the FINO 1 platform, 80 m above sea level.

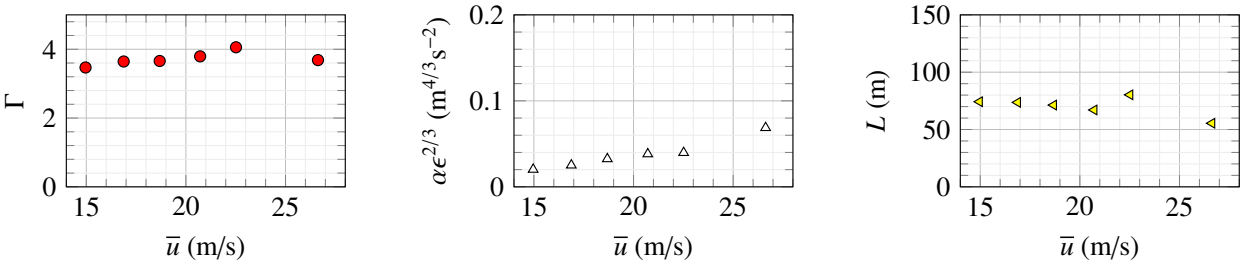

Fig. 9. Fitted coefficients for the Mann turbulence model corresponding to the spectra displayed in Fig. 8.

two other SA led to $1.8 \leq \alpha\epsilon^{2/3}z^{2/3}/u_*^2 \leq 3.0$, $15\,\mathrm{m} \leq L \leq 29\,\mathrm{m}$ and $3.0 \leq \Gamma \leq 3.1$. In the present case, we obtained $1.2 \leq \alpha\epsilon^{2/3}z^{2/3}/u_*^2 \leq 2.0$. Discrepancies may come from the different fitting methods. In the present study, the values of Γ, $\alpha\epsilon^{2/3}$ and L are simultaneously calculated by fitting the Mann turbulence model to S_u, S_v, S_w and S_{uw}. On the other hand, de Maré and Mann [22] estimated first L based on S_u and S_{uw}, and thereafter Γ and $\alpha\epsilon^{2/3}$ from S_u, S_v and S_w.

3.4. Comparison with the NORSOK spectrum and the IEC Kaimal spectrum for the along-wind component

In Fig. 10, the estimated spectra based on the FINO 1 data are compared to the IEC Kaimal spectrum and the NORSOK spectrum. Similarly to the results in Fig. 5, the IEC Kaimal spectrum shows an overall good agreement with the measured spectrum with a slight misalignment of the spectral peaks. The value of Λ_1, fixed to 42 m in Eq. 19 may be well suited for an onshore site but may be too low for the offshore environment. A value of ca. 73 m allows for example the spectral peaks of the IEC Kaimal model and of the measured spectrum to better overlap.

The Charnock coefficient is known to be estimated with a large scatter [56, 57]. Kraus and Businger [57, p. 145] report for example values ranging from 1.1×10^{-2} to 1.8×10^{-2}. This coefficient is known to be influenced by e.g. the wave age, the wave height, the water depth, the fetch [58, 59] and possibly the wind speed [60]. In the present study, two values of the Charnock coefficient were therefore investigated. The first one was $a = 0.0172$, i.e. the same value as by Andersen and Løvseth [21]. The second one was $a = 0.011$ which was proposed by Smith [16] for the open sea and adopted in IEC61400-3 [51]. For both Charnock coefficients, the spectral peak of the normalized measured spectrum and the NORSOK spectrum are relatively well aligned. However, the normalized NORSOK spectrum computed with

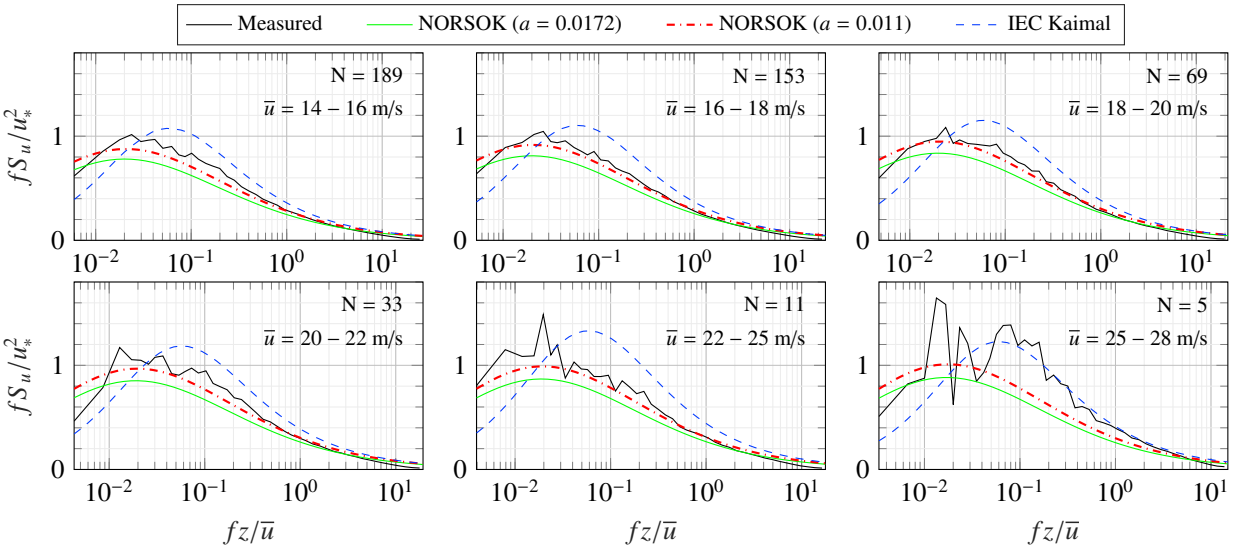

Fig. 10. Wind spectra of the along-wind component estimated based on 1 h stationary wind data recorded at the FINO 1 platform, 80 m above sea level and compared to the NORSOK spectrum and the IEC Kaimal.

$a = 0.0172$ has lower values than the measured one for $0.008 \leq n \leq 1$. For the velocity bin between $14\,\mathrm{m\,s^{-1}}$ and $16\,\mathrm{m\,s^{-1}}$, the NORSOK spectrum computed with $a = 0.0172$ is for example up to 20 % lower than the measured one. This discrepancy is greatly reduced if $a = 0.011$ is used instead. The Charnock coefficient $a = 0.011$ is consistent with the site-specific value $a = 0.012$ found by Peña and Gryning [61] in the Danish North Sea. The estimation of a site-specific Charnock coefficient at the FINO 1 platform is relevant for a more accurate comparison between the NORSOK spectrum and the measured one, but is out of the scope of the present study.

3.5. Challenges associated with the study of the surface-layer turbulence in offshore environment

The presented spectral properties of turbulence are based on the wind samples detected as stationary after removal of their fluctuating mean using the EMD [32, 34] and de-trended in an additional step. As shown in Fig. 5, the measured wind spectra still contain low-frequency components of higher magnitude than in the spectral models investigated. Similar findings have been previously reported for the horizontal turbulence [22, 62], in particular in case of non-neutral atmospheric stability. It might also explain why the wind spectra proposed by e.g. Kareem [17] or Ochi et al. [18] display a larger energy content than for onshore locations.

One of the reasons for such a larger energy content may be that the "spectral gap" [63] can be partially filled in offshore environments. The low frequency region of the microscale atmospheric motion is often assumed to be separated from the high frequency content of the larger scale convective atmospheric motion by the spectral gap [64]. For a flow from the ocean near Frøya island (where the NORSOK spectrum has been defined), Gjerstad et al. [65] and Heggem et al. [66] could not clearly identify such a spectral gap for heights above 40 m, in particular for slightly unstable and unstable conditions. The decrease of the gap depth with height was also observed by Larsén et al. [67], especially in offshore environment, where the spectral gap was almost invisible 80 m above sea level. In the present study, most of the wind samples characterized by a low-frequency spectrum larger than expected and/or a monotonically increasing wind spectrum for decreasing frequencies were discarded by removing strongly unstable or stable wind records using the method described in subsection 2.5.

Although only 20% to 30% of the wind data were observed to be non-stationary after application of the EMD and removing any linear trend, a large number of wind records were dismissed during our attempt to remove the stable and unstable conditions (from 80% in Januray 2007 to 97% in April 2008). This indicates that the wind conditions described in the present study may not be the most common ones observed at the FINO 1 platform. As observed by Archer et al. [27] in the Northeastern U.S. coast or Coelingh et al. [49] in the North Sea, an unstable stratification may

be predominant in offshore environment, which is also the atmospheric condition for which the spectral gap was not clearly observed by Gjerstad et al. [65] and Heggem et al. [66].

4. Conclusions

Two years of wind velocity data recorded from 2007 to 2008 at the FINO 1 platform in the North Sea have been used to study the spectral characteristics of offshore wind under near-neutral conditions. Wind records with an 1 h mean wind velocity ranging from 14 m s^{-1} to 28 m s^{-1} were used. Their fluctuating mean was removed using the empirical modal decomposition and their stationarity was assessed using the reverse-arrangement test. The estimated wind spectra were compared to the Kaimal spectral model, the NORSOK spectrum and the Mann turbulence model. To limit the influence of strongly unstable and stable atmospheric conditions, only samples satisfying $1.2 \leq S_w/S_u \leq 1.4$ for $2 \leq n \leq 5$ and $0.9 \leq S_w/S_u \leq 1.1$ for $0.5 \leq n \leq 1$ were selected as representative of a relatively neutral atmospheric stability.

A remarkably good agreement was obtained between the measured spectra and the Kaimal spectra for the across-wind and vertical wind components, as well as the cross-spectrum between u and w components. A good agreement was also observed for all wind velocity components analysed, down to a reduced frequency $n \simeq 0.04$. For $n \leq 0.04$, the power spectral density of the along-wind component was larger than predicted. The spectral peak of the IEC Kaimal spectrum for the along-wind component was at a somewhat higher frequency than in the present case. For the time series recorded 80 m above sea level, the IEC Kaimal spectrum can be adapted to the present data by simply increasing the longitudinal turbulence scale parameter Λ_1 from 42 m to 73 m. The NORSOK spectrum had slightly lower values than the measured ones if the Charnock coefficient a, estimated from the Sletringen data was used. A better agreement was obtained using $a = 0.011$. The Mann spectral model with parameters $\Gamma = 3.7$, $\alpha\epsilon^{2/3} = 0.04\,\mathrm{m}^{4/3}\mathrm{s}^{-2}$ and $L = 70$ m agreed well with the wind spectra measured at $z = 80$ m. Whereas Γ and L are relatively constant in the velocity range considered, $\alpha\epsilon^{2/3}$ was observed to increase from $0.02\,\mathrm{m}^{4/3}\mathrm{s}^{-2}$ at 15 m s^{-1} to $0.07\,\mathrm{m}^{4/3}\mathrm{s}^{-2}$ at ca. 27 m s^{-1}.

Acknowledgements

The FINO 1 platform is one of three offshore platforms of the FINO Project, funded by the German Federal Ministry for the Environment, Nature Conservation and Nuclear Safety (BMU). The present work was developed as a research collaboration within the Norwegian Centre for Offshore Wind Energy, (NORCOWE, Project number: 193821 supported by the Research Council Norway).

References

[1] IEC 61400-1, . IEC 61400-1 Wind turbines Part 1: Design requirements; 2005.
[2] Kaimal, J., Wyngaard, J., Izumi, Y., Coté, O.. Spectral characteristics of surface-layer turbulence. Quarterly Journal of the Royal Meteorological Society 1972;98(417):563–589. doi:10.1002/qj.49709841707.
[3] Mann, J.. The spatial structure of neutral atmospheric surface-layer turbulence. Journal of Fluid Mechanics 1994;273. doi:10.1017/s0022112094001886.
[4] NORSOK Standard, . Actions and action effects. 2007.
[5] Neumann, T., Nolopp, K., Strack, M., Mellinghoff, H., Söker, H., Mittelstaedt, E., et al. Erection of German offshore measuring platform in the North Sea. DEWI Magazin 2003;23:32–46.
[6] Türk, M., Emeis, S.. The dependence of offshore turbulence intensity on wind speed. Journal of Wind Engineering and Industrial Aerodynamics 2010;98(89):466 – 471. doi:10.1016/j.jweia.2010.02.005.
[7] Kettle, A.J.. Unexpected vertical wind speed profiles in the boundary layer over the southern North Sea. Journal of Wind Engineering and Industrial Aerodynamics 2014;134:149 – 162. doi:10.1016/j.jweia.2014.07.012.
[8] Muñoz-Esparza, D., Cañadillas, B., Neumann, T., van Beeck, J.. Turbulent fluxes, stability and shear in the offshore environment: Mesoscale modelling and field observations at FINO1. Journal of Renewable and Sustainable Energy 2012;4(6):063136. doi:10.1063/1.4769201.
[9] Emeis, S., Türk, M.. Wind-driven wave heights in the German Bight. Ocean Dynamics 2009;59(3):463–475. doi:10.1007/s10236-008-0178-x.
[10] Eliassen, L., Obhrai, C.. Coherence of turbulent wind under neutral wind conditions at FINO1. Energy Procedia 2016;94:388 – 398. doi:10.1016/j.egypro.2016.09.199.
[11] Canadillas, B., Bégué, A., Neumann, T.. Comparison of turbulence spectra derived from lidar and sonic measurements at the offshore platform FINO1. In: Proceedings of the 10th German Wind Energy Conference, DEWEK. 2010,.

[12] Cheynet, E., Bogunović Jakobsen, J., Svardal, B., Reuder, J., Kumer, V.. Wind coherence measurement by a single pulsed Doppler wind lidar. Energy Procedia 2016;94:462 – 477. doi:10.1016/j.egypro.2016.09.217.
[13] Kettle, A.J.. FINO1–research platform in the North Sea. 2013. URL: http://folk.uib.no/ake043/AJK_papers/kettle2013_litrev_fino1.pdf.
[14] Naito, G.. Direct measurements of momentum and sensible heat fluxes at the tower in the open sea. Meteorological Society of Japan, Journal 1978;56:25–34.
[15] Naito, G.. Spatial structure of surface wind over the ocean. Journal of Wind Engineering and Industrial Aerodynamics 1983;13(1-3):67–76. doi:10.1016/0167-6105(83)90129-0.
[16] Smith, S.D.. Wind stress and heat flux over the ocean in gale force winds. Journal of Physical Oceanography 1980;10(5):709–726. doi:10.1175/1520-0485(1980)010<0709:WSAHFO>2.0.CO;2.
[17] Kareem, A.. Wind-induced response analysis of tension leg platforms. Journal of Structural Engineering 1985;111(1):37–55. doi:10.1061/(ASCE)0733-9445(1985)111:1(37).
[18] Ochi, M., Shin, V., et al. Wind turbulent spectra for design consideration of offshore structures. In: Offshore Technology Conference. Offshore Technology Conference; 1988, p. 461–467. doi:10.4043/5736-MS.
[19] Andersen, O.J., Løvseth, J.. The maritime turbulent wind field. Measurements and models. Phase 2 – extension 2 - phase 4. Extended analysis of the Frøya database, ALLFORSK AVH. Tech. Rep.; Statoil technical reports from the Frya Project; 1992.
[20] Andersen, O.J., Løvseth, J.. Gale force maritime wind. The Frøya data base. Part 1: Sites and instrumentation. review of the data base. Journal of Wind Engineering and Industrial Aerodynamics 1995;57(1):97 – 109. doi:10.1016/0167-6105(94)00101-I.
[21] Andersen, O.J., Løvseth, J.. The Frøya database and maritime boundary layer wind description. Marine Structures 2006;19(23):173 – 192. doi:10.1016/j.marstruc.2006.07.003.
[22] de Maré, M., Mann, J.. Validation of theMann spectral tensor for offshore wind conditions at different atmospheric stabilities. In: Journal of Physics: Conference Series; vol. 524. IOP Publishing; 2014, p. 012106. doi:10.1088/1742-6596/524/1/012106.
[23] Teunissen, H.. Structure of mean winds and turbulence in the planetary boundary layer over rural terrain. Boundary-Layer Meteorology 1980;19(2):187–221. doi:10.1007/BF00117220.
[24] Eidsvik, K.J.. Large-sample estimates of wind fluctuations over the ocean. Boundary-Layer Meteorology 1985;32(2):103–132. doi:10.1007/BF00120931.
[25] Lumley, J.L., Panofsky, H.A.. The structure of atmospheric turbulence. John Wiley & Sons; 1964.
[26] Westerhellweg, A., Cañadillas, B., Kinder, F., Neumann, T.. Wake measurements at Alpha Ventus–Dependency on stability and turbulence intensity. In: Journal of Physics: Conference Series; vol. 555. IOP Publishing; 2014, p. 012106. doi:10.1088/1742-6596/555/1/012106.
[27] Archer, C.L., Colle, B.A., Veron, D.L., Veron, F., Sienkiewicz, M.J.. On the predominance of unstable atmospheric conditions in the marine boundary layer offshore of the US northeastern coast. Journal of Geophysical Research: Atmospheres 2016;121(15):8869–8885. doi:10.1002/2016JD024896.
[28] ESDU 86010, . Characteristics of atmospheric turbulence near the ground part III: variations in space and time for strong winds (neutral atmosphere). 2001.
[29] Xu, Y.L., Chen, J.. Characterizing nonstationary wind speed using Empirical Mode Decomposition. Journal of Structural Engineering 2004;130(6):912–920. doi:10.1061/(ASCE)0733-9445(2004)130:6(912).
[30] Chen, J., Hui, M., Xu, Y.. A comparative study of stationary and non-stationary wind models using field measurements. Boundary-layer meteorology 2007;122(1):105–121. doi:10.1007/s10546-006-9085-1.
[31] Xu, Y., Xia, Y.. Structural Health Monitoring of Long-Span Suspension Bridges. CRC Press; 2011. ISBN 9780203839669.
[32] Huang, N.E., Shen, Z., Long, S.R., Wu, M.C., Shih, H.H., Zheng, Q., et al. The empirical mode decomposition and the Hilbert spectrum for nonlinear and non-stationary time series analysis. In: Proceedings of the Royal Society of London A: Mathematical, Physical and Engineering Sciences; vol. 454. The Royal Society; 1998, p. 903–995.
[33] Bendat, J., Piersol, A.. Random Data: Analysis and Measurement Procedures. Wiley Series in Probability and Statistics; Wiley; 2011. ISBN 9781118210826.
[34] Flandrin, P., Rilling, G., Goncalves, P.. Empirical mode decomposition as a filter bank. IEEE signal processing letters 2004;11(2):112–114. doi:10.1109/LSP.2003.821662.
[35] Priestley, M.B.. Evolutionary spectra and non-stationary processes. Journal of the Royal Statistical Society Series B (Methodological) 1965;:204–237URL: http://www.jstor.org/stable/2984191.
[36] Chen, L., Letchford, C.. Numerical simulation of extreme winds from thunderstorm downbursts. Journal of Wind Engineering and Industrial Aerodynamics 2007;95(911):977 – 990. doi:10.1016/j.jweia.2007.01.021.
[37] Hu, L., Xu, Y.L., Huang, W.F.. Typhoon-induced non-stationary buffeting response of long-span bridges in complex terrain. Engineering Structures 2013;57:406–415.
[38] Wang, H., Wu, T., Tao, T., Li, A., Kareem, A.. Measurements and analysis of non-stationary wind characteristics at Sutong Bridge in Typhoon Damrey. Journal of Wind Engineering and Industrial Aerodynamics 2016;151:100 – 106. doi:10.1016/j.jweia.2016.02.001.
[39] Welch, P.D.. The use of fast Fourier transform for the estimation of power spectra: A method based on time averaging over short, modified periodograms. IEEE Trans Audio Electroacoustics 1967;15:70–73.
[40] Lynn, P.. Onshore and Offshore Wind Energy: An Introduction. Wiley; 2011. ISBN 9780470976081.
[41] Neumann, T., Nolopp, K.. Three years operation of far offshore measurements at FINO1. DEWI Mag 2007;30:42–46.
[42] Olesen, H.R., Larsen, S.E., Højstrup, J.. Modelling velocity spectra in the lower part of the planetary boundary layer. Boundary-Layer Meteorology 1984;29(3):285–312. doi:10.1007/BF00119794.
[43] Tieleman, H.W.. Universality of velocity spectra. Journal of Wind Engineering and Industrial Aerodynamics 1995;56(1):55–69. doi:10.1016/0167-6105(94)00011-2.
[44] Weber, R.. Remarks on the definition and estimation of friction velocity. Boundary-Layer Meteorology 1999;93(2):197–209. doi:10.1023/A:

1002043826623.
[45] Solari, G., Piccardo, G.. Probabilistic 3-D turbulence modeling for gust buffeting of structures. Probabilistic Engineering Mechanics 2001;16(1):73–86.
[46] Mann, J.. Wind field simulation. Probabilistic Engineering Mechanics 1998;13. doi:10.1016/s0266-8920(97)00036-2.
[47] Charnock, H.. Wind stress on a water surface. Quarterly Journal of the Royal Meteorological Society 1955;81(350):639–640. doi:10.1002/qj.49708135027.
[48] Norwegian Meteorological Institute (MET). eKlima. http://eklima.no/; 2011. Accessed: 2017-03-16.
[49] Coelingh, J., van Wijk, A., Holtslag, A.. Analysis of wind speed observations over the North Sea. Journal of Wind Engineering and Industrial Aerodynamics 1996;61(1):51 – 69. doi:10.1016/0167-6105(96)00043-8.
[50] Westerhellweg, A., Neumann, T., Riedel, V.. Fino1 mast correction. DEWI Magazin 2012;40:60–66.
[51] IEC61400-3, . Wind TurbinesPart 3: Design Requirements for Offshore Wind Turbines; 2009.
[52] Grant, A.. Observations of boundary layer structure made during the 1981 KONTUR experiment. Quarterly Journal of the Royal Meteorological Society 1986;112(473):825–841. doi:10.1002/qj.49711247314.
[53] Nicholls, S., Readings, C.. Spectral characteristics of surface layer turbulence over the sea. Quarterly Journal of the Royal Meteorological Society 1981;107(453):591–614. doi:10.1002/qj.49710745309.
[54] Simiu, E., Scanlan, R.H.. Wind effects on structures. Wiley; 1996.
[55] Sjöblom, A., Smedman, A.S.. Vertical structure in the marine atmospheric boundary layer and its implication for the inertial dissipation method. Boundary-Layer Meteorology 2003;109(1):1–25. doi:10.1023/A:1025407109324.
[56] Nordeng, T.E.. On the wave age dependent drag coefficient and roughness length at sea. Journal of Geophysical Research: Oceans 1991;96(C4):7167–7174. doi:10.1175/JAMC-D-14-0099.1.
[57] Kraus, E.B., Businger, J.A.. Atmosphere-ocean interaction; vol. 27. Oxford University Press; 1994.
[58] Taylor, P.K., Yelland, M.J.. The dependence of sea surface roughness on the height and steepness of the waves. Journal of physical oceanography 2001;31(2):572–590. doi:10.1175/1520-0485(2001)031<0572:TDOSSR>2.0.CO;2.
[59] Fairall, C., Bradley, E.F., Hare, J., Grachev, A., Edson, J.. Bulk parameterization of air–sea fluxes: Updates and verification for the coare algorithm. Journal of climate 2003;16(4):571–591. doi:10.1175/1520-0442(2003)016<0571:BPOASF>2.0.CO;2.
[60] Drennan, W.M., Taylor, P.K., Yelland, M.J.. Parameterizing the sea surface roughness. Journal of physical oceanography 2005;35(5):835–848. doi:10.1175/JPO2704.1.
[61] Peña, A., Gryning, S.E.. Charnocks roughness length model and non-dimensional wind profiles over the sea. Boundary-layer meteorology 2008;128(2):191–203. doi:10.1007/s10546-008-9285-y.
[62] Andersen, O.J., Lvseth, J.. Stability modifications of the Frøya wind spectrum. Journal of Wind Engineering and Industrial Aerodynamics 2010;98(45):236 – 242. doi:10.1016/j.jweia.2009.10.019.
[63] Van der Hoven, I.. Power spectrum of horizontal wind speed in the frequency range from 0.0007 to 900 cycles per hour. Journal of meteorology 1957;14(2):160–164. doi:10.1175/1520-0469(1957)014<0160:PSOHWS>2.0.CO;2.
[64] Fortak, H.. Meteorologie. Reimer; 1982.
[65] Gjerstad, J., Aasen, S.E., Andersson, H.I., Brevik, I., Løvseth, J.. An analysis of low-frequency maritime atmospheric turbulence. Journal of the atmospheric sciences 1995;52(15):2663–2669. doi:10.1175/1520-0469(1995)052<2663:AAOLFM>2.0.CO;2.
[66] Heggem, T., Lende, R., Løvseth, J.. Analysis of long time series of coastal wind. Journal of the atmospheric sciences 1998;55(18):2907–2917. doi:10.1175/1520-0469(1998)055<2907:AOLTSO>2.0.CO;2.
[67] Larsén, X.G., Larsen, S.E., Petersen, E.L.. Full-scale spectrum of boundary-layer winds. Boundary-Layer Meteorology 2016;159(2):349–371. doi:10.1007/s10546-016-0129-x.